Hindawi Publishing Corporation
EURASIP Journal on Wireless Communications and Networking
Volume 2006, Article ID 57018, Pages 1–16
DOI 10.1155/WCN/2006/57018

A Frame Synchronization and Frequency Offset Estimation Algorithm for OFDM System and its Analysis

Ch. Nanda Kishore[1] and V. Umapathi Reddy[1, 2]

[1] *Hellosoft India Pvt Ltd, 82 703, Road No 12, Banjara Hills, 500 034 Hyderabad, AP, India*
[2] *IIIT, Hyderabad, India*

Received 13 July 2005; Revised 12 December 2005; Accepted 19 January 2006

Recommended for Publication by Hyung-Myung Kim

Orthogonal frequency division multiplexing (OFDM) is a parallel transmission scheme for transmitting data at very high rates over time dispersive radio channels. In an OFDM system, frame synchronization and frequency offset estimation are extremely important for maintaining orthogonality among the subcarriers. In this paper, for a preamble having two identical halves in time, a timing metric is proposed for OFDM frame synchronization. The timing metric is analyzed and its mean values at the preamble boundary and in its neighborhood are evaluated, for AWGN and for frequency selective channels with specified mean power profile of the channel taps, and the variance expression is derived for AWGN case. Since the derivation of the variance expression for frequency selective channel case is tedious, we used simulations to estimate the same. Based on the theoretical value of the mean and estimate of the variance, we suggest a threshold for detection of the preamble boundary and evaluating the probability of false and correct detections. We also suggest a method for a threshold selection and the preamble boundary detection in practical applications. A simple and computationally efficient method for estimating fractional and integer frequency offset, using the same preamble, is also described. Simulations are used to corroborate the results of the analysis. The proposed method of frame synchronization and frequency offset estimation is applied to the downlink synchronization in OFDM mode of wireless metropolitan area network (WMAN) standard IEEE 802.16-2004, and its performance is studied through simulations.

1. INTRODUCTION

Orthogonal frequency division multiplexing (OFDM) is a multicarrier modulation scheme in which high rate data stream is split into a number of parallel low rate data streams, each of which modulates a separate subcarrier. Recently, OFDM has been adopted as a modulation technique in *wireless metropolitan area network* (WMAN) standard [1]. In OFDM system, timing and frequency synchronization are crucial for the retrieval of information (see [2]). If any of these tasks is not performed with sufficient accuracy, the orthogonality among the subcarriers is lost, and the communication system suffers from intersymbol interference (ISI) and intercarrier interference (ICI). Several techniques have been proposed recently for OFDM synchronization. Those suggested in [3–9] use certain structure available in the preamble while the techniques in [10, 11] propose to use the structure provided by the cyclic prefix in the data symbol. Specifically, in [10, 11], the authors exploit the correlation that exists between the samples of the cyclic prefix and the corresponding portion of the symbol. However, the number of samples that satisfy this property will be reduced by the channel impulse response length in the presence of delay spread channel. Assuming that the symbol synchronization has been achieved, Moose [3] proposed a method for estimating the frequency offset with a preamble consisting of two repeated OFDM symbols. Considering a preamble with two OFDM symbols, Schmidl and Cox proposed a method for time and frequency synchronization in [5]. Their timing metric exploits the structure in the first symbol, which consists of two identical halves in time, and it is insensitive to frequency offset and channel phase. However, the resulting metric suffers from a plateau which causes some ambiguity in determining the start of the frame. The frequency offset within ± 1 subcarrier spacing is estimated from the phase of the numerator term of the timing metric at the optimum symbol time. For

estimating the offset above ±1 subcarrier spacing, they employ the second symbol of the preamble. To avoid the ambiguity caused by the plateau of the timing metric in [5], the authors in [6, 7] proposed a preamble, consisting of consecutive copies of a synchronization pattern in time domain, and a timing metric different from that of [5]. However, in the presence of frequency selective channel, the frequency offset estimate exhibits larger variance than in the AWGN channel, even at high SNR values. The method in [8] suggests a preamble with differentially encoded time domain PN sequence for frame detection and two identical OFDM symbols for frequency offset estimation. In [4], Minn et al. designed a specific preamble, containing repetitive parts with different signs, for time and frequency synchronization. In a frequency selective channel, this repetitive structure of the received preamble is disturbed and some interference is introduced in the frequency offset estimation. They proposed to suppress this interference either by excluding those differently affected received samples from frequency offset estimation, or by finding the correct frequency estimate by maximizing another metric over all possible values of the frequency estimate around the coarse estimate. Muller-Weinfurtner [12] carried out simulations in the indoor radio communication channel environment to assess the OFDM frame synchronization performance using timing metrics of [5, 6, 10] and showed that the timing metric of [10] performs better than other timing metrics. The authors in [9] have proposed an m-sequence (maximum length shift register sequence) based frame synchronization method for OFDM systems. An m-sequence is added directly to the OFDM signal at the beginning of the frame at the transmitter and the autocorrelation property of m-length sequence is exploited at the receiver to find the frame boundary estimate. Wu and Zhu [13] proposed a method of frame and frequency synchronization for OFDM systems using a preamble consisting of two symbols, which is the same as the one recommended for the OFDM mode of WMAN [1]. The first symbol of the preamble has four identical parts and they used Schmidl and Cox timing metric [5] during this symbol for initial timing. The second symbol has conjugate symmetry and they exploit this property to achieve an accurate frame boundary estimation. The fractional frequency offset is found using the repetitive structure of the preamble. After the fractional part of the frequency offset is compensated, the integer frequency offset is found by maximizing a correlation function for all possible values.

In this paper, a timing metric is proposed for OFDM frame synchronization using an OFDM symbol with two identical parts in time domain as a preamble. This preamble is the same as the second symbol of the downlink preamble suggested for the OFDM mode in WMAN [1]. Later we show that this method can be extended to a preamble having four identical parts. Considering an ideal scenario, we show that the metric yields a sharp peak at the correct symbol boundary. The metric is analyzed and its mean values at the symbol boundary and in its neighborhood are evaluated for AWGN and frequency selective channels with specified mean power profile of the channel taps, and the variance of the metric is derived for AWGN case. Since the derivation of the variance expression for frequency selective channel case is tedious, we use simulations to estimate this. Based on the mean values and variances, we select a threshold for detection of the symbol boundary and evaluate the probability of false and correct detections. A method for selecting a threshold and a detection strategy in practical applications is also suggested. A simple and computationally efficient method for estimating fractional and integer frequency offset is described. The proposed timing and frequency synchronization methods are applied to the downlink synchronization in the OFDM mode of WMAN, IEEE 802.16-2004. Simulations are provided to illustrate the performance of the proposed methods and also to support the results of analysis. The rest of the paper is organized as follows.

Section 2 briefly describes the basics of the underlying OFDM system. In Section 3, the proposed timing metric is motivated for the ideal channel with no noise. Section 4 analyses the proposed timing metric for the AWGN and frequency selective channels. The mean values of the timing metric are evaluated at exact symbol boundary and in its neighborhood for AWGN and frequency selective channels, and the variance is derived for AWGN channel (in the appendix) while it is estimated for SUI channels using simulations. Selection of threshold and evaluation of the probability of false and correct detections are discussed in this section. A detection strategy for practical applications is also described in this section. Section 5 presents a simple and computationally efficient frequency offset estimation algorithm. In Section 6, we apply the frame synchronization and frequency offset estimation algorithms to the OFDM mode in WMAN and present the results. Section 7 concludes the paper.

2. A TYPICAL OFDM SYSTEM

The block diagram of a typical OFDM transmitter is shown in Figure 1. A block of input data bits is first encoded and interleaved. The interleaved bits are then mapped to PSK or QAM subsymbols, each of which modulates a different carrier. Known pilot symbols modulate pilot subcarriers. The pilots are used for estimating various parameters. The subsymbols for the guard carriers are zero amplitude symbols. The cyclic prefix of length L, which is longer than the channel impulse response length, is appended at the beginning of the OFDM symbol. The baseband OFDM signal is generated by taking the inverse fast Fourier transform (IFFT) [14] of the PSK or QAM subsymbols.

The samples of the baseband equivalent OFDM signal can be expressed as

$$x(n) = \frac{1}{\sqrt{N}} \sum_{k=0}^{N-1} X(k) e^{j2\pi k(n-L)/N}, \quad 0 \le n \le N+L-1, \quad (1)$$

where N is the total number of carriers, $X(k)$ is the kth subsymbol, and $j = \sqrt{-1}$. The signal is transmitted through a frequency selective multipath channel. Let $h(n)$ denote the baseband equivalent discrete-time channel impulse response

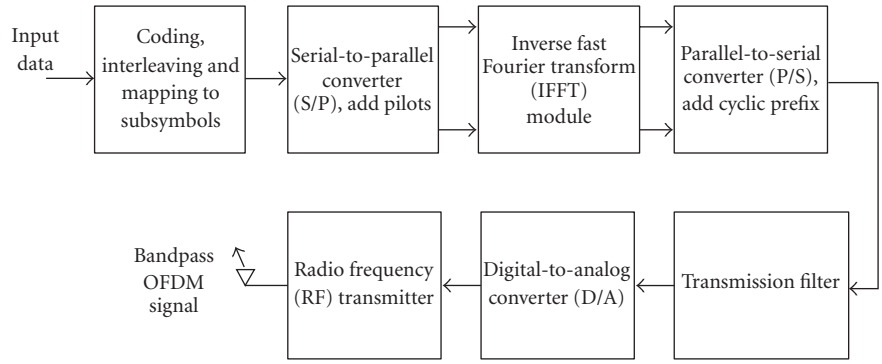

Figure 1: Block diagram of an OFDM transmitter.

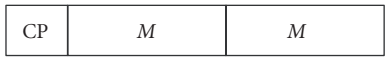

Figure 2: Preamble (preceded by CP) considered for the proposed timing synchronization.

of length v. A carrier frequency offset of ϵ (normalized with subcarrier spacing) causes a phase rotation of $2\pi\epsilon n/N$. Assuming a perfect sampling clock, the received samples of the OFDM symbol are given by

$$r(n) = e^{j[(2\pi\epsilon n/N)+\theta_0]} \sum_{l=0}^{v-1} h(l)x(n-l) + \eta(n), \tag{2}$$

where θ_0 is an initial arbitrary carrier phase and $\eta(n)$ is a zero mean complex white Gaussian noise with variance σ_η^2. In this paper, we consider packet-based OFDM communication system, where preamble is placed at the beginning of the packets. The frame boundary, which is the same as the preamble boundary, is estimated using the timing synchronization algorithm. The frequency offset is estimated using the frequency offset estimation algorithm. The received OFDM symbol needs to be compensated for the frequency offset before proceeding with demodulation.

3. PROPOSED TIMING METRIC

Consider an OFDM symbol preceded by CP as shown in Figure 2. The two halves of this symbol are made identical (in time domain) by loading even carriers with a pseudo-noise (PN) sequence. If the length of CP is at least as large as that of channel impulse response, then the two halves of the symbol remain identical at the output of the channel, except for a phase difference between them due to carrier frequency offset. Considering this symbol as a preamble, and prompted from the WMAN-OFDM mode preamble [1], where the loaded PN sequence is specified a priori, we propose the following timing metric for frame synchronization:

$$M(d) = \frac{|P(d)|^2}{R^2(d)}, \tag{3}$$

where $P(d)$ and $R(d)$ are given by

$$P(d) = \sum_{i=0}^{M-1} \left[r(d+i)a(i)\right]^* \left[r(d+i+M)a(i)\right], \tag{4}$$

$$R(d) = \sum_{i=0}^{M-1} |r(d+i+M)|^2. \tag{5}$$

The superscript "$*$" denotes complex conjugation, $M = N/2$ with N denoting the symbol length, $r(n)$ are the samples of the baseband equivalent received signal, and d is a sample index of the first sample in a window of $2M$ samples. $R(d)$ gives an estimate of the energy in M samples of the received signal. The samples $a(n)$ for $n = 0, 1, \ldots, M-1$ are the transmitted time domain samples in one half of the preamble which are assumed to be known to the receiver. Note that the metric here is different from that of [5] and the difference is in the numerator term $P(d)$ which uses transmitted time domain samples $a(n)$ unlike in [5]. We now give some motivation for the above metric.

To keep the exposition simple, assume an ideal channel with no noise. Then, samples of the received preamble (preceded by CP) are

$$r(n) = e^{j[2\pi\epsilon n/N+\theta_0]} \times a\big((n-L) \bmod M\big), \quad n = 0, 1, \ldots, 2M+L-1. \tag{6}$$

The product obtained by multiplying the conjugate of one sample from first half with the corresponding sample from the second half of the received symbol will have a phase $\phi = \pi\epsilon$. Consider the case where d corresponds to a sample in the interval consisting of CP and the left boundary of the preamble. Without loss of generality, let d denote the sample index measured with respect to left boundary of the CP. That is, $d = 0$ implies that the window of $2M$ samples begins at the left boundary of the CP. Then, for $0 \le d \le L$, (4) can be expressed as

$$P(d) = e^{j\phi} \sum_{i=0}^{M-1} a^*\big((d+i-L) \bmod M\big) \times a\big((d+i+M-L) \bmod M\big) |a(i)|^2 \tag{7}$$

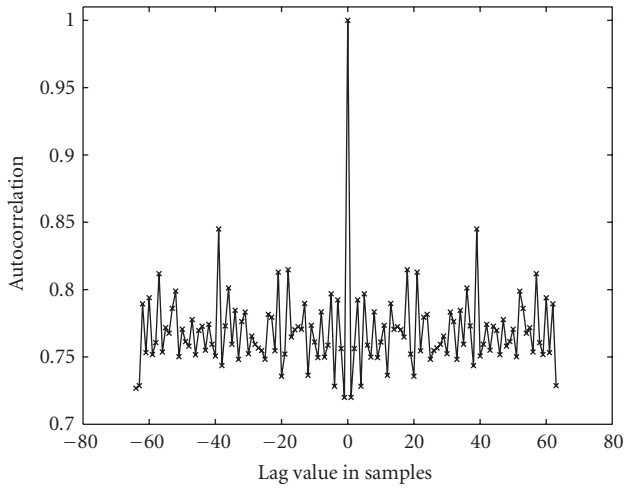

Figure 3: Normalized autocorrelation $(G(\tau)/G(0))$ of the sequence $|a(i)|^2$.

which simplifies to

$$P(d) = e^{j\phi} \sum_{i=0}^{M-1} \left| a\left((d+i-L) \bmod M\right) \right|^2 \left| a(i) \right|^2 = e^{j\phi} G(d-L), \tag{8}$$

where $G(\tau)$ denotes cyclic autocorrelation of the sequence $|a(i)|^2$ for lag τ. Since $G(\tau)$ has a peak at $\tau = 0$ (see Figure 3), the magnitude of $P(d)$ attains maximum value when $d = L$. From (5) and (6), for $0 \le d \le L$, $R(d)$ is given by

$$R(d) = \sum_{i=0}^{M-1} \left| a\left((d+i+M-L) \bmod M\right) \right|^2 = \sum_{i=0}^{M-1} \left| a(i) \right|^2. \tag{9}$$

Since $R(d)$ remains constant for all the values of d under consideration and $|P(d)|$ attains maximum value when $d = L$, the metric (3) will attain a peak value when the left boundary of the window aligns with the left boundary of the preamble. The relative value of this peak compared to those for $d \neq L$ depends on the nature of the autocorrelation $G(\tau)$. Figure 3 shows the plot of $G(\tau)$, normalized with respect to its peak value $G(0)$, for the case when the samples $a(i)$ are generated by loading the even subcarriers of the preamble with a PN sequence (in frequency domain) as specified in [1] for OFDM mode. The shape of the autocorrelation plot suggests that the proposed metric will yield a sharp peak at the correct symbol boundary.

4. ANALYSIS OF THE PROPOSED TIMING METRIC

Recall that the samples of the transmitted preamble (preceded by CP) are $a((n-L) \bmod M)$ for $n = 0, 1, \ldots, 2M + L - 1$. Let $r(n) = s(n) + \eta(n)$ be the samples of the received preamble where $s(n)$ is the signal part (for $0 \le n \le 2M + L - 1$) given by

$$s(n) = \begin{cases} e^{j[(2\pi\epsilon n/N)+\theta_0]} a\left((n-L) \bmod M\right) & \text{AWGN channel,} \\ e^{j[(2\pi\epsilon n/N)+\theta_0]} & \\ \quad \times \sum_{l=0}^{v-1} h(l) a\left((n-L-l) \bmod M\right) & \text{FSC,} \end{cases} \tag{10}$$

and $\eta(n)$ is the noise part (FSC = frequency selective channel). Let $r_1(n) = r^*(n) r(n+M) = s_1(n) + \eta_1(n)$, where

$$s_1(n) = s^*(n) s(n+M), \tag{11}$$

$$\eta_1(n) = s^*(n)\eta(n+M) + s(n+M)\eta^*(n) + \eta^*(n)\eta(n+M). \tag{12}$$

Now, consider $P(d)$ given in (4). Recall that d is a sample index of the first sample in a window of $2M$ received samples, measured with respect to the left boundary of CP. Using the above notation, we can express $P(d)$ as

$$P(d) = \sum_{i=0}^{M-1} s_1(d+i) \left| a(i) \right|^2 + \sum_{i=0}^{M-1} \eta_1(d+i) \left| a(i) \right|^2. \tag{13}$$

Assume that d corresponds to a sample index in the interval spanning the ISI-free portion of CP and the preamble boundary. For these values of d, $s_1(d+i)$ has a phase $\phi = \pi\epsilon$. The $P(d)$ given in (13) can be broken into parts that are in-phase and quadrature phase to $s_1(d+i)$, similar to that given in [5]. For moderate values of SNR, the magnitude of the quadrature part is small compared to that of in-phase part and can be neglected [5]. Then, $|P(d)|$ can be expressed as

$$\left| P(d) \right| = e^{-j\phi} \sum_{i=0}^{M-1} \Big(s_1(d+i) \left| a(i) \right|^2 + \text{inPhase}_\phi \{ \eta_1(d+i) \} \left| a(i) \right|^2 \Big), \tag{14}$$

where $\text{inPhase}_\phi\{U\}$ denotes the component of U in the ϕ direction. From (5), the estimate of the received signal energy is

$$R(d) = \sum_{i=0}^{M-1} \Big(|s(d+i+M)|^2 + |\eta(d+i+M)|^2 + 2\,\text{Re}\{s^*(d+i+M)\eta(d+i+M)\}\Big). \tag{15}$$

From the *Central limit theorem*, both $|P(d)|$ and $R(d)$ are Gaussian distributed. From (10), (11), and (14), $|P(d)|$ simplifies to zero lag cyclic autocorrelation of $|a(i)|^2$ for $d = L$ in the case of ideal channel with no noise. On the other hand, the metric of [5] remains constant for all values of d in the interval under consideration leading to a plateau.

Consider the square root of the timing metric $Q(d) = \sqrt{M(d)}$. Numerator and denominator of $Q(d)$ are Gaussian random variables. If the standard deviations of both these random variables are much smaller than their mean values, then the mean and the variance of $Q(d)$ are obtained as [15] (using the first-order terms in Taylor series expansion of the ratio $|P(d)|/R(d)$),

$$\mu_{Q(d)} = E[Q(d)] = \frac{E[\,|P(d)|\,]}{E[R(d)]}, \tag{16}$$

$$\sigma^2_{Q(d)} = \frac{\sigma^2_{|P(d)|} + \mu^2_{Q(d)}\sigma^2_{R(d)} - 2\mu_{Q(d)}\,\text{cov}\,(|P(d)|, R(d))}{(E[R(d)])^2}, \tag{17}$$

where $E[\cdot]$ denotes expectation operator, $\sigma^2_{Q(d)}$, $\sigma^2_{|P(d)|}$, and $\sigma^2_{R(d)}$ represent variances of $Q(d)$, $|P(d)|$, and $R(d)$, respectively, and $\text{cov}(|P(d)|, R(d))$ is the covariance between $|P(d)|$ and $R(d)$.

Under the condition that $E[|P(d)|]$ is much larger than its standard deviation, and similarly for $R(d)$, the ratio $Q(d)$ can be expressed as $Q(d) = \mu_{Q(d)} + \zeta(0, \sigma^2_{Q(d)})$, where $\zeta(\mu, \sigma^2)$ denotes a Gaussian random variable with mean μ and variance σ^2. Then, $M(d)$ can be approximated as

$$M(d) = [\mu_{Q(d)} + \zeta(0, \sigma^2_{Q(d)})]^2 \approx \mu^2_{Q(d)} + 2\mu_{Q(d)}\zeta(0, \sigma^2_{Q(d)}). \tag{18}$$

In (18), it is assumed that $\mu_{Q(d)}$ is much larger than $\sigma^2_{Q(d)}$, which is valid in view of the assumptions[1] made regarding the means and variances of $|P(d)|$ and $R(d)$. Thus, we have the mean and variance of $M(d)$ as

$$\mu_{M(d)} = \mu^2_{Q(d)}, \tag{19}$$

$$\sigma^2_{M(d)} = 4\mu^2_{Q(d)}\sigma^2_{Q(d)}. \tag{20}$$

We now derive the expression for the mean value of the timing metric for AWGN and frequency selective channels.

[1] These assumptions are verified using simulations.

4.1. AWGN channel

Using (10) and (11), we can write $s_1(i)$ as

$$s_1(i) = e^{j\phi}\,|a((i-L) \bmod M)|^2. \tag{21}$$

Substituting (21) in (14), we get

$$|P(d)| = \sum_{i=0}^{M-1} |a((d+i-L) \bmod M)|^2\,|a(i)|^2 + \sum_{i=0}^{M-1} \text{inPhase}_\phi\{\eta_1(d+i)\}\,|a(i)|^2. \tag{22}$$

Since the expectation of the second term in (22) is zero,

$$E[\,|P(d)|\,] = \sum_{i=0}^{M-1} |a((d+i-L) \bmod M)|^2\,|a(i)|^2 = G(d-L). \tag{23}$$

From (10) and (15), we have

$$R(d) = \sum_{i=0}^{M-1} \Big(|a((d+i-L) \bmod M)|^2 + |\eta(d+i+M)|^2 + 2\,\text{Re}\{a^*((d+i-L) \bmod M)\eta(d+i+M)\}\Big), \tag{24}$$

and taking expectation, we obtain

$$E[R(d)] = \sum_{i=0}^{M-1} \Big[\,|a(i)|^2 + \sigma^2_\eta\Big] = \mathcal{E}_a + M\sigma^2_\eta, \tag{25}$$

where $\mathcal{E}_a$ is the energy in one half of the preamble and σ^2_η is the variance of the noise $\eta(n)$. Combining (23) and (25) with (16) and (19) gives the mean value of the timing metric as

$$\mu_{M(d)} = \frac{[G(d-L)]^2}{[\mathcal{E}_a + M\sigma^2_\eta]^2}. \tag{26}$$

The numerator term in (26) is square of the lag $(d-L)$ cyclic autocorrelation of the sequence $|a(i)|^2$. Since the denominator term remains constant for all values of d under consideration, which in the case of AWGN correspond to the whole interval of CP and the preamble boundary, the mean value of the timing metric will attain maximum value for $d = L$. From the autocorrelation of $|a(i)|^2$, shown in Figure 3, the mean value at the correct symbol boundary $(d = L)$ is at least 1.4 times the mean value at any other time instant in the CP interval.

The expression for variance of the timing metric is derived in the appendix.

4.2. Frequency selective channel

For the frequency selective channel case, using (10) and (11), we can express $s_1(i)$ as

$$\begin{aligned} s_1(i) = e^{j\phi} \sum_{l=0}^{v-1} |h(l)|^2 |a((i-L-l) \bmod M)|^2 \\ + \sum_{l=0}^{v-1} \sum_{m=l+1}^{v-1} 2\,\mathrm{Re}\{h^*(l)h(m)a^*((i-L-l) \bmod M) \\ \times a((i-L-m) \bmod M)\}. \end{aligned} \tag{27}$$

Substituting (27) into (14) gives

$$\begin{aligned} &|P(d)| \\ &= \sum_{i=0}^{M-1} \sum_{l=0}^{v-1} |h(l)|^2 |a((d+i-L-l) \bmod M)|^2 |a(i)|^2 \\ &\quad + \sum_{i=0}^{M-1} \mathrm{inPhase}_\phi\{\eta_1(d+i)\} |a(i)|^2 \\ &\quad + \sum_{i=0}^{M-1} \sum_{l=0}^{v-1} \sum_{m=l+1}^{v-1} 2\,\mathrm{Re} \\ &\qquad \{h^*(l)h(m)a^*((d+i-L-l) \bmod M) \\ &\qquad \times a((d+i-L-m) \bmod M)\} |a(i)|^2. \end{aligned} \tag{28}$$

Here, d is assumed to correspond to a sample index in the interval spanning the ISI-free portion of CP and the preamble boundary, that is, $v \le d \le L$. The value of v is obtained from the mean power profile of the channel taps, which is normally specified for a multipath channel.

The expectation of the second term in (28) is zero and the expectation of the third term will also be zero if we assume the channel taps to be zero mean complex Gaussian random variables that are mutually uncorrelated. Then, the mean value of $|P(d)|$ is given by (after interchanging the summations)

$$\begin{aligned} &E[|P(d)|] \\ &\quad = \sum_{l=0}^{v-1} \rho_l \left[\sum_{i=0}^{M-1} |a((d+i-L-l) \bmod M)|^2 |a(i)|^2 \right] \\ &\quad = \sum_{l=0}^{v-1} \rho_l G(d-L-l), \end{aligned} \tag{29}$$

where $\rho_l = E[|h(l)|^2]$ is the power in lth tap.

The estimate of the signal energy in one half of the preamble can be expressed as

$$\begin{aligned} R(d) = &\sum_{i=0}^{M-1} \sum_{l=0}^{v-1} |h(l)|^2 |a(i)|^2 \\ &+ \sum_{i=0}^{M-1} \sum_{l=0}^{v-1} \sum_{m=l+1}^{v-1} 2\,\mathrm{Re}\{h^*(l)h(m) \\ &\qquad \times a^*((d+i-L-l) \bmod M) \\ &\qquad \times a((d+i-L-m) \bmod M)\} \\ &+ \sum_{i=0}^{M-1} 2\,\mathrm{Re}\left\{ \sum_{l=0}^{v-1} h^*(l)a^*((d+i-L-l) \bmod M) \right. \\ &\qquad \left. \times \eta(d+i+M) \right\} \\ &+ \sum_{i=0}^{M-1} |\eta(d+i+M)|^2, \end{aligned} \tag{30}$$

and its mean as

$$\begin{aligned} E[R(d)] &= \sum_{i=0}^{M-1} \sum_{l=0}^{v-1} \rho_l |a(i)|^2 + \sum_{i=0}^{M-1} \sigma_\eta^2 \\ &= \rho \mathcal{E}_a + M\sigma_\eta^2, \end{aligned} \tag{31}$$

where $\rho = \sum_{l=0}^{v-1} \rho_l$. Combining (29) and (31) with (16) and (19), we obtain

$$\mu_{M(d)} = \frac{\left[\sum_{l=0}^{v-1} \rho_l G(d-L-l)\right]^2}{\left[\rho \mathcal{E}_a + M\sigma_\eta^2\right]^2}. \tag{32}$$

The numerator term is square of the convolution of the sequence of tap powers with the sequence $G(\tau - L)$. Since the denominator term remains constant for all the values of d under consideration, the mean value of the timing metric in the interval $v \le d \le L$ is determined by the numerator term only which depends on the nature of cyclic autocorrelation of $|a(i)|^2$ and the distribution of the channel tap powers.

Since the derivation of the variance expression in the case of frequency selective channel is tedious, we use simulations to estimate this.

4.3. Simulations

To see if the mean of the timing metric evaluated above, using certain assumptions, is useful in practice, we use simulations to verify this and also to estimate the variance of the timing metric, which is later used in evaluating probability of false and correct detections.

The preamble is generated with 200 used carriers, 56 null carriers −28 on the left and 27 on the right, and a dc carrier. The even (used) carriers are loaded with a PN sequence given in [1] for OFDM mode. A frequency offset of 10.5 times the

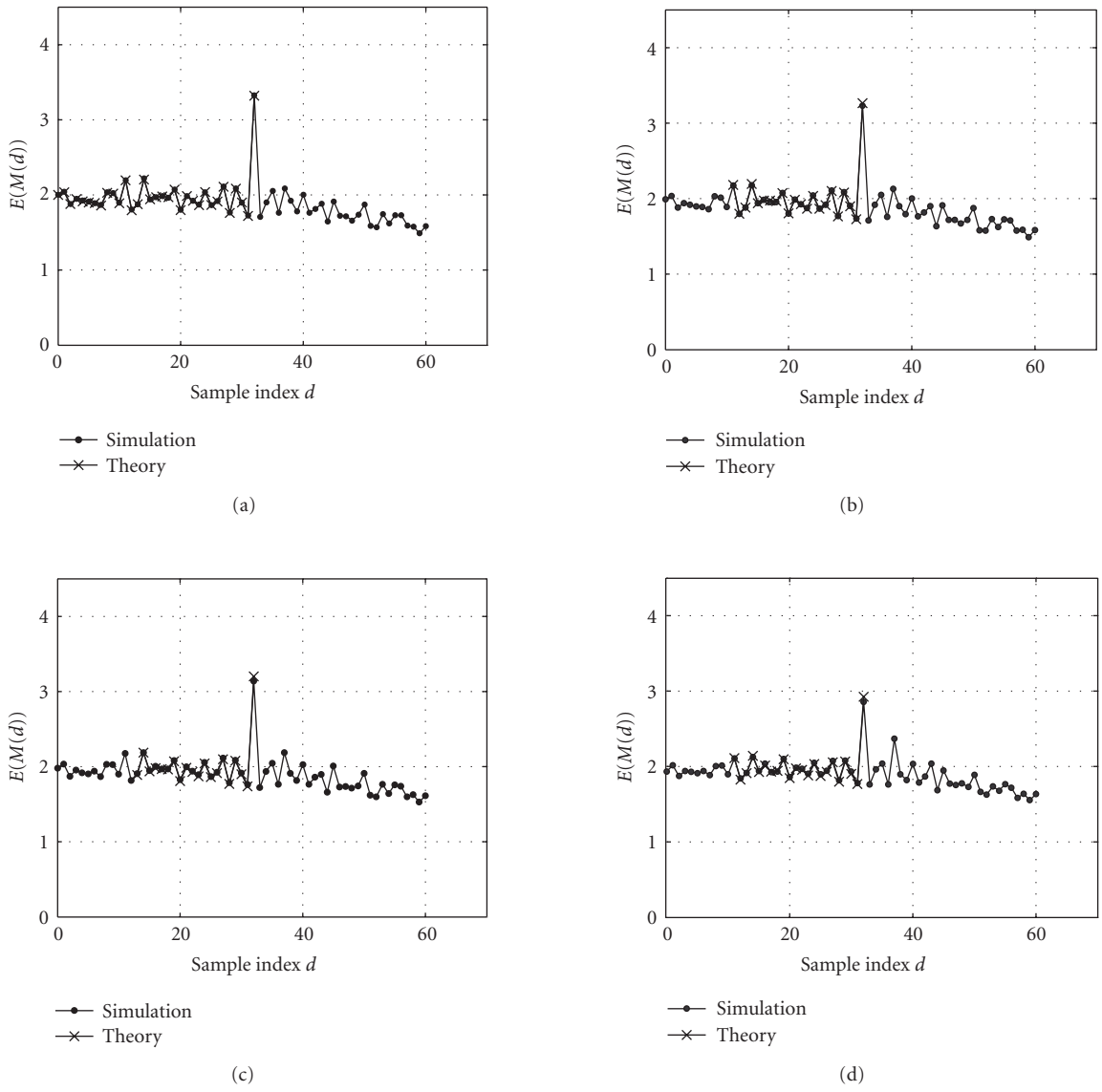

Figure 4: Mean of the timing metric as a function of the sample index d: (a) AWGN, (b) SUI-1, (c) SUI-2, (d) SUI-3 (SNR = 9.4 dB and $d = 0$ corresponds to the left edge of the CP).

subcarrier spacing and a cyclic prefix of length 32 samples are assumed in the simulations. Stanford University interim (SUI) channel modeling [16] is used to simulate a frequency selective channel. The impulse response of the channel is normalized to unit norm. Variance of the zero mean complex white Gaussian noise, which is added to the signal component, is adjusted according to the required SNR. An SNR of 9.4 dB is assumed in the simulations as the recommended SNR of the preamble [1]. The received signal generated as above is preceded by noise and followed by data symbols. The timing metric given in (3), (4), and (5) is applied to a block of $2M$ samples of the received signal, shifting the block by one sample index each time, and $M(d)$ is computed. This is repeated 1000 times, choosing a different noise realization each time in the AWGN case, and choosing a different realization of noise and the channel each time in the SUI channel case. From the 1000 values of $M(d)$, we estimated the mean and variance of $M(d)$.

The mean of the metric evaluated from the analytical expressions ((26) for the AWGN and (32) for the SUI channel), and the corresponding values estimated from the simulations are shown in Figure 4. For AWGN case, the analytical expression is evaluated in the interval $0 \le d \le L$, while in the case of SUI channels, the corresponding expression is evaluated in the interval $v \le d \le L$. The mean power profile of the channel taps for SUI channels gave $v = 11, 13$, and 11 for SUI-1, SUI-2, and SUI-3, respectively (with a sampling rate of 11.52 MHz). The same mean power profile is used in evaluating (32). The sequence $a(i)$ is determined from the IFFT output by loading the even subcarriers of the preamble with a PN sequence given in [1], and its cyclic autocorrelation is computed.

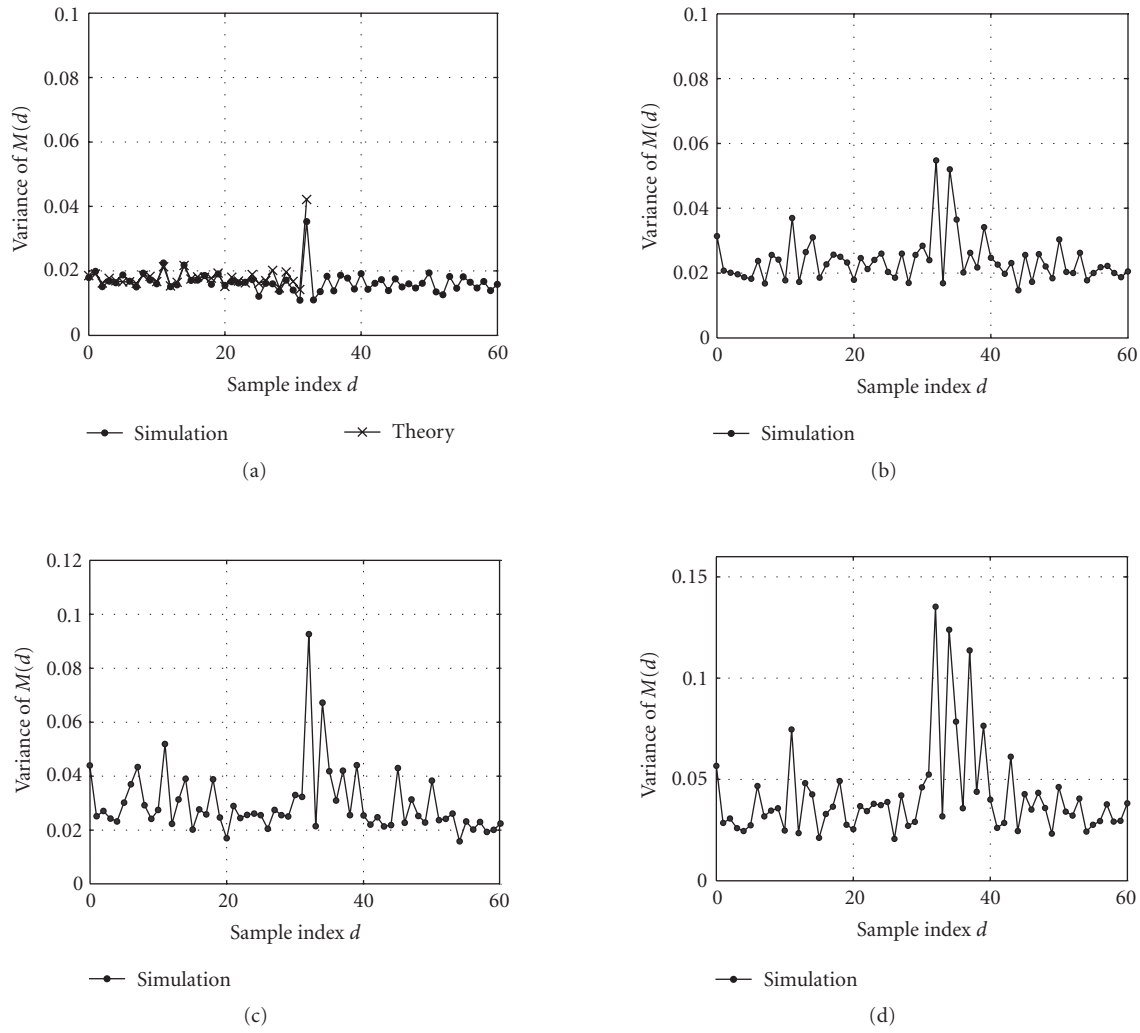

Figure 5: Variance of the timing metric as a function of the sample index d: (a) AWGN, (b) SUI-1, (c) SUI-2, (d) SUI-3 (SNR = 9.4 dB and $d = 0$ corresponds to the left edge of the CP).

The variance of the timing metric is shown in Figure 5, where the analytical result is given for AWGN case only. We note the following from the plots of Figures 4 and 5.

(i) The theoretically predicted value of the mean of $M(d)$ is very close to the value estimated from the simulations.

(ii) The variance of $M(d)$ is significantly smaller than its mean in the interval where the analysis applies, particularly for AWGN, SUI-1, and SUI-2 channels. In the case of AWGN, the variance predicted by theory is close to the value estimated from the simulations.

(iii) The mean value of the metric outside the interval of interest (i.e., outside the ISI-free portion of CP and the preamble boundary) is significantly smaller than that at the preamble boundary, in particular for AWGN, SUI-1, and SUI-2 channels.

The inferences made under (i) and (ii) suggest that the assumptions made in the analysis are valid. We now suggest a threshold and evaluate probability of false and correct detection for the selected threshold.

4.4. Threshold selection and probability of false and correct detection

We observe from the plots of Figure 4 that the peak at $d = L = 32$ is the largest, and for $d < L$ there is a second largest peak at $d = 14$. We choose the threshold as $M_{th} = \mu_{M(14)} + 2\sigma_{M(14)}$. Since the timing metric $M(d)$ is Gaussian distributed with mean $\mu_{M(d)}$ and variance $\sigma^2_{M(d)}$, probability that the second largest peak exceeds the above threshold is given by

$$\Pr\left(M(14) > M_{th}\right) = \frac{1}{\sqrt{2\pi}\sigma_{M(14)}} \times \int_{M_{th}}^{\infty} e^{-(M(14)-\mu_{M(14)})^2/2\sigma^2_{M(14)}} dM(14) \tag{33}$$

Table 1: Detection performance of the proposed timing metric (Number of trials = 1000, SNR = 9.4 dB).

Channel	M_{th}	Theory		Simulations	
		P_{false}	P_{correct}	P_{false}	P_{correct}
AWGN	2.4979	0.0596	0.9403	0.0570	0.9424
SUI-1	2.5279	0.0569	0.9422	0.0750	0.9230
SUI-2	2.5606	0.0585	0.9195	0.0600	0.9010
SUI-3	2.5216	0.0931	0.7248	0.1270	0.7000

Table 2: Detection performance of the proposed metric with practical detection strategy (Number of trials = 1000, SNR = 9.4 dB, $M_{th} = 2.4979$).

Channel type	Miss detections	False detections	Correct detections
AWGN	0	0	1000
SUI-1	2	2	996
SUI-2	34	14	952
SUI-3	171	78	751

which simplifies to

$$\Pr\left(M(14) > M_{th}\right) = Q\left(\frac{M_{th} - \mu_{M(14)}}{\sigma_{M(14)}}\right), \tag{34}$$

where $Q(x) = (1/\sqrt{2\pi})\int_x^\infty e^{-y^2/2}dy$. Since $\mu_{M(11)}$ is nearly equal to $\mu_{M(14)}$ (see Figure 4), we have to consider the false detections that occur at $d = 14$ and $d = 11$. Since all other peaks, for $d < L$, are significantly smaller than these two peaks, we do not consider those peaks in the calculation of probability of false detection. Thus, the probability of false detection is approximately equal to

$$P_{\text{false}} \approx Q\left(\frac{M_{th} - \mu_{M(14)}}{\sigma_{M(14)}}\right) + Q\left(\frac{M_{th} - \mu_{M(11)}}{\sigma_{M(11)}}\right). \tag{35}$$

The probability of correct detection is then given by

$$P_{\text{correct}} = Q\left(\frac{M_{th} - \mu_{M(32)}}{\sigma_{M(32)}}\right) - P_{\text{false}}. \tag{36}$$

We evaluated the probabilities of false and correct detections using (35) and (36) for AWGN and SUI channels, and the results are shown in Table 1. The corresponding values obtained using simulations are also shown in the table. As before, we repeated the simulation experiment 1000 times using a different realization of noise and channel each time. In each trial of the simulation, we computed $M(d)$ and found the sample index d, say d^{th}, where $M(d)$ exceeds the threshold M_{th}. If this time index is L, we declare the detection as the correct detection (recall that d is measured with respect to the left edge of the CP and $d = 0$ corresponds to this edge). If it is not L, we declare the detection as false detection. There may be cases where $M(d)$ does not exceed the threshold in the search interval $0 \le d \le L$, in which case we declare the detection as miss detection.

We note from Table 1 that the simulation results are close to those predicted by theory for AWGN case. In the case of SUI channels, the probability of false detection obtained from simulation is higher than that predicted by theory and consequently the probability of correct detection yielded by simulation is lower than that given by theory. This is because, in the case of SUI channels, the variance of the timing metric for values of d other than $d = 14$ and $d = 11$ is significantly large when compared to the values at $d = 11$ and 14 and this might have caused additional false detections at the corresponding values of d. In the case of SUI-3 channel, the probability of correct detection has dropped significantly because, we have not considered the cases where timing estimate shifts due to channel dispersion (where magnitude of the second or/and third taps becomes largest), and in those cases, the timing estimate should be preadvanced by some samples to maintain the orthogonality among the subcarriers [4]. We have observed channel dispersion more significantly in SUI-3 channel.

4.5. Threshold selection and detection strategy in practical applications

In the previous subsection, we selected a threshold for detection of the preamble boundary, and the sample index where the timing metric crosses the threshold is taken as the estimate of the preamble boundary. The threshold was different for different channels. In practice, however, we should select a threshold and detection strategy that works well for all channels and for SNRs above the lowest operating value. For practical applications, we suggest the following detection strategy using the threshold selected for AWGN case in the previous subsection.[2]

(i) Compute the timing metric $M(d)$ from a block of N received samples, shifting the block by one sample index each time and find the sample index d^{th} where $M(d)$ crosses the threshold.
(ii) Evaluate $M(d)$ in the interval $d^{th} < d \le (d^{th} + L - 1)$.
(iii) Find the sample index where $M(d)$ is the largest in the interval $d^{th} \le d \le (d^{th} + L - 1)$. This sample index is taken as the estimate of the preamble boundary.
(iv) If the metric $M(d)$ does not cross the threshold at all, declare the detection as a miss, detection.

Using the above detection strategy, we repeated the simulation experiment 1000 times as before, and determined the number of false, miss, and correct detections. The results are tabulated in Table 2.

We note from Table 2 that the practical detection strategy yields higher correct detections compared to the scheme used in earlier subsection. As explained earlier, the lower number of correct detections in the SUI-3 channel is because we have

[2] In the case of AWGN, the mean and variance of the metric, in the interval $0 \le d \le L$, can be computed analytically.

Table 3: Detection performance of Schmidl and Cox metric [5] (Number of trials = 1000, SNR = 9.4 dB).

Channel type	False detections	Correct detections
AWGN	32	968
SUI-1	51	949
SUI-2	78	922
SUI-3	83	917

not considered the cases where the preamble boundary estimate shifts due to the channel dispersion.

4.6. Detection performance of Schmidl and Cox method [5]

Since the preamble of Figure 2 is the same as that considered in [5], it would be interesting to compare the performance of our method with that of [5]. The simulation experiment is repeated as before and the sample index corresponding to the symbol boundary is estimated as outlined in [5], which is described below for the sake of completeness.

We computed the sample index where the metric of [5] attains maximum value, which we denote as $d_{\max}$, and determined the sample indexes, one on the right and another on the left of $d_{\max}$, where the metric attains 90% of the value at $d_{\max}$. Then, the sample index, which is average of the two sample indexes determined as above, is taken as the estimate of the symbol boundary. If this time index falls in the ISI-free portion of CP, we declare it as a correct detection. Otherwise, we declare it as a false detection. Table 3 gives the results obtained from 1000 Monte Carlo runs. Comparing the results of this table with those of Table 2, we note that Schmidl and Cox method [5] yields fewer correct detections in AWGN, SUI-1, and SUI-2 channels, while it performs better in SUI-3 channel.

We may point out here that to obtain a sample index on the left of $d_{\max}$ where the metric attains 90% of the value at $d_{\max}$, we have to begin the metric computation from a sample index much earlier than the left boundary of the CP. This is, however, not practical since the metric computation is normally performed after energy detection which normally occurs in the CP interval. Hence, the results given here can be viewed as optimistic.

5. FREQUENCY OFFSET ESTIMATION

The frequency offset is estimated after frame synchronization. This task involves estimation of both fractional and integer parts of the frequency offset. In this section, we describe the frequency offset estimation algorithm using the preamble shown in Figure 2.

5.1. Decomposition of the offset into fractional and integer parts

In the presence of frequency offset ϵ, the samples of the received symbol (see (2)) will have a phase term of the form $[2\pi\epsilon n/N+\theta_0]$. The phase angle of $P(d)$ at the symbol boundary, in the absence of noise, is $\phi = \pi\epsilon$. Therefore, if the frequency offset is less than a subcarrier spacing ($|\epsilon| < 1$), it can be estimated from

$$\hat{\phi} = \text{angle}\,(P(d_{\text{opt}})), \tag{37}$$

$$\hat{\epsilon} = \hat{\phi}/\pi, \tag{38}$$

where d_{opt} is the estimate of sample index corresponding to the preamble boundary and $\hat{\epsilon}$ is the estimate of the frequency offset. If, on the other hand, the actual frequency offset is more than a subcarrier spacing, say $\overline{\epsilon} = m + \delta$ with $m \in \mathcal{Z}$ and $|\delta| < 1$, then the frequency offset estimated from (38) will be the estimate of

$$\epsilon = m + \delta - \overline{m}, \tag{39}$$

where $\overline{m}$ represents an even integer closest to $\overline{\epsilon}$. Here, ϵ corresponds to the fractional part, and $\overline{m}$ is the even integer since the repeated halves of the preamble are the result of loading the even subcarriers with nonzero value and odd subcarriers with zero value. After compensating the received preamble with fractional frequency offset, $\overline{m}$ is estimated from the bin shift, as described in the next subsection. The total frequency offset estimate is the sum of the estimate of the fractional part and the bin shift.

5.2. Bin shift estimation

Let $r(d_{\text{opt}} + n)$, $n = 0, 1, \ldots, N-1$, be the received OFDM symbol where $N = 2M$ denotes the length of the OFDM symbol (excluding CP). This sequence is first compensated with the fractional frequency offset estimate $\hat{\epsilon}$ as follows:

$$c(n) = e^{-j2\pi\hat{\epsilon}n/N} r(d_{\text{opt}} + n), \quad n = 0, 1, \ldots, N-1. \tag{40}$$

Let

$$C(k) = \frac{1}{\sqrt{N}} \sum_{i=0}^{N-1} c(i) e^{-j2\pi ki/N}, \quad k = 0, 1, \ldots, N-1,$$

$$A(k) = \frac{1}{\sqrt{N}} \sum_{i=0}^{N-1} a(i \bmod M) e^{-j2\pi ki/N}, \quad k = 0, 1, \ldots, N-1 \tag{41}$$

be the DFTs of the received and transmitted symbols, respectively. Since PN sequence is loaded on the even subcarriers only for the preamble, $A(k)$ is zero for odd values of k. The cross-correlation $R_{\text{AC}}(l)$ of $A(k)$ and $C(k)$ for lag l is given by

$$R_{\text{AC}}(l) = \sum_{k=0}^{N-1} C(k) A^*(k-l). \tag{42}$$

The lag corresponding to the largest (in magnitude) value of $R_{\text{AC}}(l)$ gives the desired bin shift. Rather than evaluating (42) for all even values of l, we suggest below a computationally efficient method.

Since a bin shift estimate is an even integer, consider the cross-correlation for even lag values

$$\begin{aligned} R_{\mathrm{AC}}(2l) &= \sum_{k=0}^{N-1} C(k)A^*(k-2l) \\ &= \sum_{k=0}^{M-1} C(2k)A^*(2k-2l), \quad 0 \le l \le M-1, \end{aligned} \tag{43}$$

where the last step in (43) follows from the fact that $A(k)$ is zero for odd values of k. Substituting (41) in (43), we get

$$\begin{aligned} R_{\mathrm{AC}}(2l) = \frac{1}{N} \sum_{k=0}^{M-1} \sum_{i=0}^{N-1} c(i) e^{-j4\pi ki/N} \\ \times \sum_{m=0}^{N-1} a^*(m \bmod M) e^{j4\pi(k-l)m/N}. \end{aligned} \tag{44}$$

Interchanging the summations and simplifying, we obtain

$$R_{\mathrm{AC}}(2l) = \frac{1}{2} \sum_{i=0}^{N-1} c(i) a^*(i \bmod M) e^{-j4\pi li/N}. \tag{45}$$

Let $c(n) = s(n) + \eta'(n)$, $n = 0, 1, \ldots, N-1$, where $s(n)$, given by

$$s(n) = \begin{cases} e^{j[(2\pi(\epsilon-\hat{\epsilon})n/N)+\theta]} a(n \bmod M) & \text{AWGN channel,} \\ e^{j[(2\pi(\epsilon-\hat{\epsilon})n/N)+\theta]} & \\ \quad \times \sum_{m=0}^{v-1} h(m) a((n-m) \bmod M) & \text{FSC,} \end{cases} \tag{46}$$

represents the signal component and $\eta'(n)$[3] represents the white noise component. The constant phase θ is the sum of θ_0, initial arbitrary carrier phase, and the phase accumulated up to the sample index d_{opt}, $2\pi\epsilon d_{\mathrm{opt}}/N$. Assuming that the variance of the error in the fractional frequency offset estimate is small, we can write $s(n+M) \approx s(n)$ for $0 \le n \le M-1$. Then, (45) can be expressed as

$$\begin{aligned} R_{\mathrm{AC}}(2l) = \sum_{i=0}^{M-1} s(i) a^*(i) e^{-j4\pi li/N} \\ + \frac{1}{2} \sum_{i=0}^{N-1} \eta'(i) a^*(i \bmod M) e^{-j4\pi li/N} \end{aligned} \tag{47}$$

which can be simplified to

$$\begin{aligned} R_{\mathrm{AC}}(2l) = \sum_{i=0}^{M-1} c(i) a^*(i) e^{-j2\pi li/M} \\ + \frac{1}{2} \sum_{i=0}^{M-1} [\eta'(i+M) - \eta'(i)] a^*(i) e^{-j2\pi li/M}. \end{aligned} \tag{48}$$

[3] $\eta'(n)$ is same as $\eta(n)$ except for the phase term $e^{-j2\pi\hat{\epsilon}n/N}$.

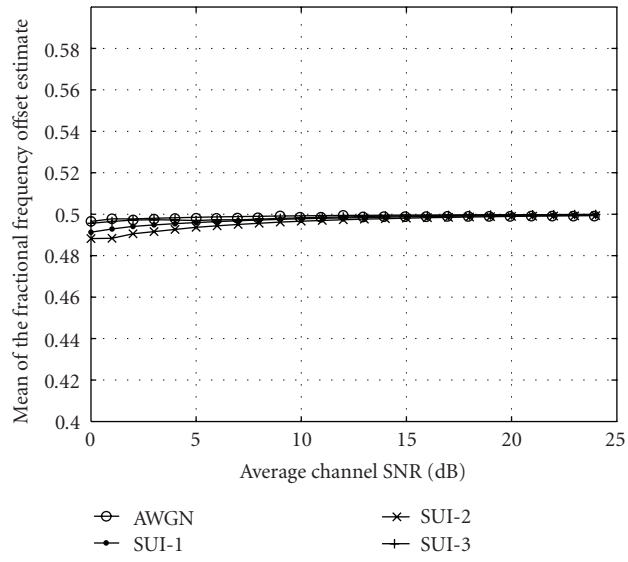

Figure 6: Mean of the fractional frequency offset estimate (frequency offset = 10.5).

Since the signal is correlated with $a(i)$ and uncorrelated with the noise, magnitude of the second term in (48) will be very small compared to that of the first term, and therefore, can be neglected. Thus, (48) can be approximated as

$$R_{\mathrm{AC}}(2l) \approx \sum_{i=0}^{M-1} c(i) a^*(i) e^{-j2\pi li/M}. \tag{49}$$

Note that (49) is the M-point DFT of the product sequence $c(n)a^*(n)$ for $n = 0, 1, \ldots, M-1$, except for the normalization factor. Thus, the algorithm for estimating the bin shift reduces to the following.

(i) Compute the samples $c(n)$, $n = 0, 1, \ldots, M-1$, using (40).
(ii) Obtain the product sequence $c(n)a^*(n)$.
(iii) Evaluate the M-point DFT of the product sequence obtained in step (ii).
(iv) Find the bin l_1, corresponding to the DFT coefficient whose magnitude is the largest. Then, $2l_1$ is the estimate of the bin shift.

To illustrate how the frequency offset estimation algorithm performs in both AWGN and frequency selective channels, we have performed simulations with 1000 different realizations of channel and noise. As before, we assumed a frequency offset of 10.5 in the simulations. From the results of 1000 trials, we computed mean and variance of the fractional frequency offset estimate. We repeated the simulations for different values of SNR and the results are shown in Figures 6 and 7.

Note from the results of Figure 7 that the variance of the fractional frequency offset estimate is smaller than 2×10^{-4} for SNRs beyond 5 dB in all the cases (AWGN and SUI channels). Combining this with the results of mean (see Figure 6), we observe that the fractional frequency offset estimate is

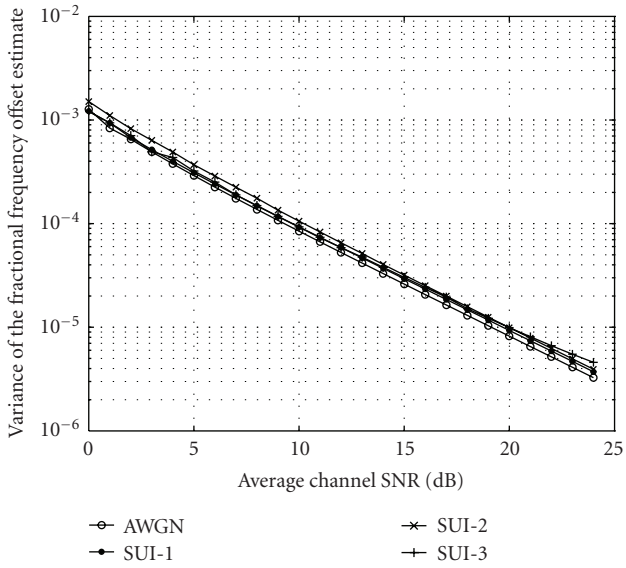

Figure 7: Variance of the fractional frequency offset estimate (frequency offset = 10.5).

very close to the true value for SNRs beyond 5 dB in AWGN and SUI-1 channels, and for SNRs beyond 10 dB in SUI-2 and SUI-3 channels. For the realizations in which the estimate of the preamble boundary was correct, the integer frequency offset estimate was 10 in the case of AWGN, SUI-1, and SUI-2 channels for SNRs above 0 dB. In the case of SUI-3 channel, out of the runs in which the estimate of the preamble boundary was correct, the integer frequency offset estimate was 10 in 94% of the runs for SNR = 0 dB and 98% of the runs for SNR = 10 dB.

6. APPLICATION OF THE PROPOSED SYNCHRONIZATION TECHNIQUES TO WIRELESS MAN

The IEEE 802.16-2004 standard [1] specifies the air interface of a fixed point to multipoint broadband wireless access system providing multiple services in a WMAN. The standard includes a particular physical layer specification applicable to systems operating between 2 GHz and 11 GHz, and between 10 GHz and 66 GHz. The 10–66 GHz air interface, based on a single-carrier modulation, is known as the WMAN-SC air interface. The 2–11 GHz air interface includes WirelessMAN-SCa, WirelessMAN-OFDM, WirelessMAN-OFDMA, and WirelessHUMAN. In this section, the synchronization algorithms, described in the previous sections, are applied to downlink synchronization in WirelessMAN-OFDM. First, we describe the preamble structure specified for WirelessMAN-OFDM mode.

6.1. Preamble structure in WMAN-OFDM mode

The WMAN-OFDM physical layer is based on the OFDM modulation with 256 subcarriers. For this mode, the preamble consists of two OFDM symbols. Each of these symbols is preceded by a cyclic prefix (CP), whose length is the same as that for data symbols. In the first OFDM symbol, only the subcarriers whose indices are multiple of 4 are loaded. As a result, the time domain waveform (IFFT output) of the first symbol consists of 4 repetitions of 64-sample fragment. In the second OFDM symbol, only the even subcarriers are loaded which result in a time domain waveform consisting of 2 repetitions of 128-sample fragment. The corresponding preamble structure is shown in Figure 8. During initialization, a subscriber station should search for all possible values of CP and find the value that is used by the base station.

CP	64	64	64	64	CP	128	128

Figure 8: Downlink preamble structure in OFDM mode of WMAN.

6.2. Downlink synchronization

In the downlink synchronization in the WMAN-OFDM case, we have to estimate the symbol boundary, frequency offset, and the CP value using the preamble given in Figure 8. To evaluate the CP value, we estimate the left edge of one of the 64-sample segments and the left edge of the second symbol. Since the first symbol has 4 identical segments, we first compute the timing metric with a window of length $N/2$ samples, and hence, the sample index corresponding to the largest value of the timing metric (as outlined in Section 4.5) gives an estimate of the left edge of one of the first three segments. Then, we estimate the frequency offset, apply the correction and proceed with the detection of the left edge of the second symbol using a window of length N samples.

The first symbol of the preamble, shown in Figure 8, has four identical parts in time and the timing metric described in Section 3 is used with the following modifications:

$$M_1(d) = \frac{|P_1(d)|^2}{R_1^2(d)}, \tag{50}$$

where $P_1(d)$ and $R_1(d)$ are given by

$$\begin{aligned} P_1(d) &= \sum_{i=0}^{N/4-1} [r(d+i)a_1(i)]^* [r(d+i+N/4)a_1(i)], \\ R_1(d) &= \sum_{i=0}^{N/4-1} |r(d+i+N/4)|^2. \end{aligned} \tag{51}$$

Here, d is a sample index corresponding to the first sample in a window of $N/2$ samples. $R_1(d)$ gives an estimate of the energy in $N/4$ samples of the received signal. The samples $a_1(n)$, $n = 0, 1, \ldots, N/4 - 1$, are the transmitted time domain samples in one segment of the first symbol, which are assumed to be known to the receiver.

The timing metric (50) is analogous to the timing metric (3), and it is easy to show that its mean will attain maximum value for $d = L, L + N/4, L + N/2$ in the case of AWGN channel, where d is the sample index measured with respect to left

boundary of CP of the first symbol. Following the analysis in Section 4, we determine mean and variance of $M_1(d)$ for the first symbol of the preamble, at an SNR of 9.4 dB, for AWGN case and select a threshold as M_{th} = Mean(second peak) + 2 Std(second peak), where Std(x) denotes the standard deviation of x, and use the practical detection strategy described in Section 4.5 with the timing metric $M_1(d)$ and detect the left edge of one of the first three segments. In the presence of frequency offset ϵ_1, if the conjugate of a sample in one segment is multiplied with the corresponding sample in the next segment, the product will have a phase $\phi_1 = \pi\epsilon_1/2$. Thus, the frequency offset within 2 subcarrier spacings ($|\epsilon_1| < 2$) can be estimated from

$$\widehat{\phi_1} = \text{angle}\,(P_1(d_{\text{seg}})), \tag{52}$$

$$\widehat{\epsilon_1} = 2\widehat{\phi_1}/\pi, \tag{53}$$

where d_{seg} is the estimate of sample index corresponding to the left edge of one of the first three segments. If the actual frequency offset is more than 2 subcarrier spacings, say $\overline{\epsilon_1} = z + \gamma$ with $z \in \mathcal{Z}$ and $|\gamma| < 2$, then the frequency offset estimated from (53) will be the estimate of

$$\epsilon_1 = z + \gamma - \overline{z}, \tag{54}$$

where $\overline{z}$ represents an integer multiple of 4 closest to $\overline{\epsilon_1}$. We can apply the bin estimation algorithm here to estimate the integer frequency offset following steps given in Section 5. But the number of samples that would be used in the estimation here will be smaller than what we would have after detecting the boundary of the second symbol of the preamble. We therefore defer this estimation to the next symbol.

After estimating $\widehat{\epsilon_1}$, we apply the correction to the received samples starting from the sample index where computation of $M_1(d)$ ended, and compute the timing metric $M(d)$, given in (3), (4), and (5), with a window of length N. We use the practical detection strategy described in Section 4 for the detection of the left edge of the second symbol. Since this symbol has two repetitions of 128-sample block, the residual fractional frequency offset is estimated from (38). The integer frequency offset (bin shift) is estimated following the steps given in Section 5.2.

The CP length is estimated from

$$\widehat{L} = Q[\,(d_2 - d_1 - 1) \bmod 64], \tag{55}$$

where d_1 is the estimate of the left edge of one of the first three segments of the first symbol, and d_2 is the estimate of the left boundary of the second symbol. The function $Q(x)$ denotes the quantization of x to the nearest value among 0 (or 64), 8, 16, and 32, corresponding to CP lengths of 64, 8, 16, and 32, respectively.

6.3. Simulations

The performance of the proposed synchronization algorithms, when applied to OFDM mode of WMAN, is studied through simulations. The simulation setup is the same as the one described in Section 4.3 except that the preamble shown in Figure 8 is employed.

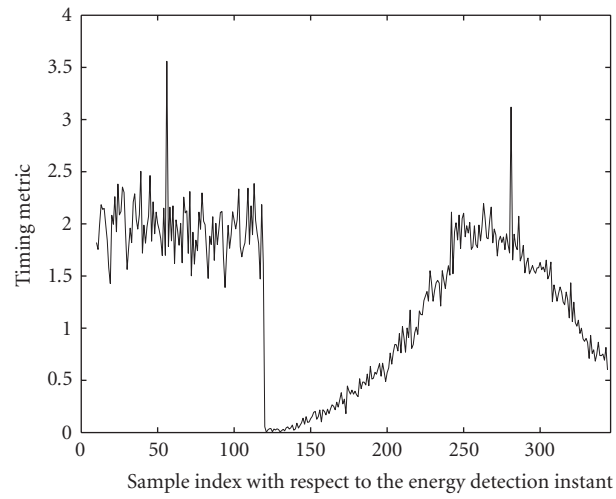

Figure 9: Timing metric during first and second symbols of the preamble for SUI-1 channel (SNR = 9.4 dB, 10 samples are left for AGC after energy detection).

The downlink synchronization starts with energy detection of the received signal. After energy detection, few samples, say 10, are left for AGC (automatic gain control) purpose. Then, we applied the timing metric $M_1(d)$ to a block of $N/2$ received samples, shifting the block by one sample each time, and followed the detection strategy described in Section 4.5, choosing the search interval equal to the largest possible CP length. The initial portion of Figure 9 shows the plot of $M_1(d)$ for one realization of SUI-1 channel. Note that $d = 0$ corresponds to the sample index where the energy of the received signal is detected and 10 samples are left for AGC purpose. From Figure 9, the peak value of $M_1(d)$ is at $d = d_1 = 56$, and this sample index corresponds to the left edge of the second segment of the first symbol of the preamble. We estimated the fractional frequency offset ϵ_1 from (53) and applied correction to the received samples from the sample index where the computation of $M_1(d)$ ended.

Next, we applied the timing metric $M(d)$, to a block of N received samples, from the sample index where the computation of $M_1(d)$ ended, shifting the block by one sample each time, and followed the detection strategy described above. The second portion of Figure 9 shows the plot of $M(d)$ for one realization of SUI-1 channel. The peak value of $M(d)$ is at $d = d_2 = 281$, which corresponds to the left edge of the second symbol of the preamble. For this example, the CP length estimated from (55) was 32, which is equal to the true value. We then computed the residual frequency offset estimate using (38). After compensating the second received symbol with the residual frequency offset, we estimated the integer frequency offset estimate following the steps given in Section 5.2.

To evaluate the effectiveness of our method on the detection of symbol boundary, CP length estimation, fractional and integer frequency offset estimation, we repeated the simulation experiment 1000 times choosing a different realization of noise and channel each time. Table 4 gives the results

Table 4: Detection performance of the proposed method in OFDM mode of WMAN (Number of trials = 1000, SNR = 9.4 dB).

Channel type	Miss detections	False detections	Correct detections	Correct CP length estimation
AWGN	0	0	1000	1000
SUI-1	8	1	991	992
SUI-2	38	22	940	958
SUI-3	171	127	702	813

on symbol detection and CP estimation, and Table 5 gives the mean and variance of the fractional and residual frequency offset estimate, obtained during the first and second symbols, respectively.

Comparing the results of Table 4 with those of Table 2, we note that the number of correct detections has come down slightly in WMAN-OFDM mode. This may be due to the larger search interval we used in the latter case[4] since the CP length is not known a priori in WMAN-OFDM mode. The number of times the CP length was estimated correctly is more than the number of correct symbol boundary detections, particularly in SUI-2 and SUI-3 channels. This is possible because of the way we estimated the CP length (see (55)). Since the CP length used in the simulations was 32, with an error of less than 16 samples in the detections of symbol boundary, segment edge, or combination of both, the CP length estimate will be correct.

Table 5 shows the results of mean and variance of fractional and residual frequency offset estimates, obtained during first and second symbols, respectively. We note that the fractional frequency offset derived during the first symbol of the preamble is very close to the true value. Further, for the realizations in which the estimate of the preamble boundary was detected correctly, the integer frequency offset estimate was correct in 100% of the runs in the case of AWGN, SUI-1, and SUI-2 channels, and 98% of the runs in the case of SUI-3 channel.

7. CONCLUSIONS

Frame synchronization and frequency offset estimation are very important in the design of a robust OFDM receiver. If any of these tasks is not performed with sufficient accuracy, orthogonality among the subcarriers will be lost and intersymbol interference and intercarrier interference will be introduced. In this paper, a new method of frame synchronization is presented for the OFDM systems using a preamble having two identical parts in time. The proposed method is robust to frequency offset and channel phase. Considering an ideal scenario, it is shown that the proposed metric yields a sharp peak at the preamble boundary. The metric is analyzed and its mean and variance at the preamble boundary and in its neighborhood are evaluated for the case of AWGN and frequency selective channels. Based on the mean and variance of the timing metric in the neighborhood of the preamble boundary, a threshold is selected and probabilities of false and correct detections are evaluated. We have also suggested a method for a threshold selection and the preamble boundary detection in practical applications. Simulation results agree closely with those of theory. A simple and computationally efficient method for estimating the frequency offset is also described using the same preamble, and its performance is studied through simulations.

The proposed method of frame synchronization and frequency offset estimation is applied to synchronization in OFDM mode of IEEE 802.16-2004 WMAN in the downlink and its performance is illustrated through simulations.

[4] The search interval was 64 while the CP length used in the simulation was 32.

APPENDIX

VARIANCE EXPRESSION FOR THE AWGN CHANNEL CASE

In this appendix, the expression for the variance of the timing metric for AWGN channel case is derived using formulas (17) and (20).

Let $\alpha(n) = [2\pi\epsilon n/N] + \theta_0$ and $\beta(n) = \text{angle}(a(n \bmod M))$ for $0 \le n \le N-1$. Expanding $\eta_1(d+i)$ in (22) using (10) and (12), $|P(d)|$ can be written as

$$\begin{aligned}|P(d)| = \sum_{i=0}^{M-1} \Big(& |a((d+i-L) \bmod M)|^2 |a(i)|^2 \\ & + |a((d+i-L) \bmod M)|\,|a(i)|^2 \text{inPhase}_\phi \\ & \{e^{j[\alpha(d+i)-\beta(d+i)]}\eta(d+i+M)\} \\ & + |a((d+i-L) \bmod M)|\,|a(i)|^2 \text{inPhase}_\phi \\ & \{e^{j[\alpha(d+i)+\beta(d+i)]}\eta^*(d+i)\} + |a(i)|^2 \\ & \times \text{inPhase}_\phi\{\eta^*(d+i)\eta(d+i+M)\}\Big).\end{aligned} \tag{A.1}$$

Here, $\eta^*(d+i)$ and $\eta(d+i+M)$ are zero mean white Gaussian random variables with variance σ_η^2, and multiplication of these variables by a complex exponential of unit magnitude will not change their variance. Therefore, from (A.1), the variance of $|P(d)|$ is given by

$$\sigma_P^2(d) = \sum_{i=0}^{M-1} |a(i)|^4 \left[|a((d+i-L) \bmod M)|^2 \sigma_\eta^2 + \frac{\sigma_\eta^4}{2} \right]. \tag{A.2}$$

From (15) and (10), $R(d)$ can be written as

$$\begin{aligned}R(d) = \sum_{i=0}^{M-1} \Big(& |a((d+i+M) \bmod M)|^2 + |\eta(d+i+M)|^2 \\ & + 2|a((d+i-L) \bmod M)| \\ & \times \text{Re}\{e^{j[\alpha(d+i)-\beta(d+i)]}\eta(d+i+M)\}\Big).\end{aligned} \tag{A.3}$$

Table 5: Frequency offset estimation performance in OFDM mode of WMAN (actual frequency offset = 10.5, number of trials = 1000, SNR = 9.4 dB).

Channel type	Fractional frequency offset estimation during the first symbol		Residual frequency offset estimation during the second symbol	
	Mean	Variance	Mean	Variance
AWGN	−1.5008	8.72×10^{-4}	7.6×10^{-4}	9.88×10^{-4}
SUI-1	−1.5006	8.44×10^{-4}	8.48×10^{-4}	9.68×10^{-4}
SUI-2	−1.5000	9.57×10^{-4}	-2.7×10^{-4}	0.0011
SUI-3	−1.5002	8.86×10^{-4}	5.97×10^{-4}	0.001

The variance of $R(d)$ is given by

$$\begin{aligned}\sigma^2_{R(d)} &= \sum_{i=0}^{M-1} \left(\sigma^4_\eta + 2\left|a((d+i-L) \bmod M)\right|^2 \sigma^2_\eta\right) \\ &= M\sigma^4_\eta + 2\mathcal{E}_a\sigma^2_\eta.\end{aligned} \tag{A.4}$$

Note from (A.4) that $\sigma^2_{R(d)}$ is constant for all values of d under consideration ($0 \le d \le L$). From (A.1) and (A.3), the covariance between $|P(d)|$ and $R(d)$ is given by

$$\begin{aligned}&\operatorname{cov}\left(|P(d)|, R(d)\right) \\ &= 2E\Bigg[\sum_{l=0}^{M-1}\sum_{m=0}^{M-1} |a(l)|^2 \left|a((d+l-L) \bmod M)\right| \\ &\qquad \times \left|a((d+m-L) \bmod M)\right| \text{inPhase}_\phi \\ &\qquad \{e^{j[\alpha(d+l)-\beta(d+l)]}\eta(d+l+M)\} \\ &\qquad \times \text{Re}\left\{e^{j[\alpha(d+m)-\beta(d+m)]}\eta(d+m+M)\right\}\Bigg].\end{aligned} \tag{A.5}$$

Note that $\text{inPhase}_\phi\{U\} = \text{Re}\{e^{j\phi}U\}$ and the noise is assumed to be complex white Gaussian with variance σ^2_η. Then, (A.5) can be simplified as

$$\operatorname{cov}\left(|P(d)|, R(d)\right) = \sum_{l=0}^{M-1} |a(l)|^2 \left|a((d+l-L) \bmod M)\right|^2 \sigma^2_\eta. \tag{A.6}$$

From (23), (25), and (16), the mean value of $Q(d)$ can be written as

$$\mu_{Q(d)} = \frac{\sum_{i=0}^{M-1} \left|a((d+i-L) \bmod M)\right|^2 |a(i)|^2}{\mathcal{E}_a + M\sigma^2_\eta}. \tag{A.7}$$

Substituting (A.2), (A.4), and (A.6) in (17), variance of $Q(d)$ can be obtained as

$$\begin{aligned}\sigma^2_{Q(d)} &= \frac{1}{\left[\mathcal{E}_a + M\sigma^2_\eta\right]^2} \\ &\quad \times \sum_{i=0}^{M-1} \left\{|a(i)|^4 \left[\left|a((d+i-L) \bmod M)\right|^2 \sigma^2_\eta + \frac{\sigma^4_\eta}{2}\right]\right. \\ &\qquad + \mu^2_{Q(d)}\left[M\sigma^4_\eta + 2\mathcal{E}_a\sigma^2_\eta\right] - 2\mu_{Q(d)}|a(i)|^2 \\ &\qquad \left. \times \left|a((d+i-L) \bmod M)\right|^2 \sigma^2_\eta\right\}.\end{aligned} \tag{A.8}$$

The variance of $M(d)$ is obtained by substituting (A.8) in (20),

$$\begin{aligned}\sigma^2_{M(d)} &= \frac{4\mu^2_{Q(d)}}{\left[\mathcal{E}_a + M\sigma^2_\eta\right]^2} \\ &\quad \times \sum_{i=0}^{M-1} \left\{|a(i)|^4 \left[\left|a((d+i-L) \bmod M)\right|^2 \sigma^2_\eta + \frac{\sigma^4_\eta}{2}\right]\right. \\ &\qquad + \mu^2_{Q(d)}\left[M\sigma^4_\eta + 2\mathcal{E}_a\sigma^2_\eta\right] - 2\mu_{Q(d)}|a(i)|^2 \\ &\qquad \left. \times \left|a((d+i-L) \bmod M)\right|^2 \sigma^2_\eta\right\}.\end{aligned} \tag{A.9}$$

ACKNOWLEDGMENTS

Ch. Nanda Kishore would like to thank S. Rama Rao, Vice-President and Dr. Y. Yoganandam, Senior Technical Director of Hellosoft India Pvt. Ltd. for their encouragement and support extended during the course of this work. Part of this work was presented at 2004 International Conference on Signal Processing and Communications (SPCOM-2004), December 2004, Bangalore, India.

REFERENCES

[1] *Part 16: Air Interface for Fixed Broadband Wireless Access Systems*, IEEE Std. 802.16, 2004.

[2] M. Speth, S. A. Fechtel, G. Fock, and H. Meyr, "Optimum receiver design for wireless broadband systems using OFDM—part 1," *IEEE Transactions on Communications*, vol. 47, no. 11, pp. 1668–1677, 1999.

[3] P. Moose, "A technique for orthogonal frequency division multiplexing frequency offset correction," *IEEE Transactions on Communications*, vol. 42, pp. 2908–2914, 1994.

[4] H. Minn, V. Bhargava, and K. Letaief, "A robust timing and frequency synchronization for OFDM systems," *IEEE Transactions on Wireless Communications*, vol. 2, pp. 822–839, 2003.

[5] T. Schmidl and D. Cox, "Robust frequency and timing synchronization for OFDM," *IEEE Transactions on Communications*, vol. 45, pp. 1613–1621, 1997.

[6] T. Keller and L. Hanzo, "Orthogonal frequency division multiplex synchronization techniques for wireless local area networks," in *Proceedings of 7th IEEE International Symposium on Personal, Indoor and Mobile Radio Communications (PIMRC '96)*, pp. 963–967, Taipei, Taiwan, October 1996.

[7] T. Keller, L. Piazzo, P. Mandarini, and L. Hanzo, "Orthogonal frequency division multiplex synchronization techniques for

frequency-selective fading channels," *IEEE Journal on Selected Areas in Communications*, vol. 19, no. 6, pp. 999–1008, 2001.

[8] T. Haiyun, K. Lau, and R. Brodersen, "Synchronization schemes for packet OFDM system," in *Proceedings of IEEE International Conference on Communications (ICC '03)*, vol. 5, pp. 3346–3350, Anchorage, Alaska, USA, May 2003.

[9] J. L. Zhang, M. Z. Wang, and W. L. Zhu, "A novel OFDM frame synchronization scheme," in *Proceedings of IEEE International Conference on Communications, Circuits and Systems and West Sino Expositions*, vol. 1, pp. 119–123, New York, NY, USA, July 2002.

[10] J.-J. van de Beek, M. Sandell, and P. O. Börjesson, "ML estimation of timing and frequency offset in multicarrier systems," Tech. Rep. TULEA 1996:09, Lulea University of Technology, Division of Signal Processing, Lulea, Sweden, April 1996.

[11] J.-J. van de Beek, M. Sandell, M. Isaksson, and P. O. Börjesson, "Low-complex frame synchronization in OFDM systems," in *Proceedings of IEEE International Conference on Universal Personal Communication (ICUPC '95)*, pp. 982–986, Tokyo, Japan, November 1995.

[12] S. H. Muller-Weinfurtner, "On the optimality of metrics for coarse frame synchronization," in *Proceedings of 9th IEEE International Symposium on Personal Indoor and Mobile Radio Communications (PIMRC '98)*, pp. 533–537, Boston, Mass, USA, September 1998.

[13] M. Wu and W.-P. Zhu, "A preamble aided symbol and frequency synchronization scheme for OFDM systems," in *Proceedings of IEEE International Symposium on Circuits and Systems (ISCAS '05)*, pp. 2627–2630, Kobe, Japan, May 2005.

[14] S. B. Weinstein and P. M. Ebert, "Data transmission by frequency division multiplexing using the discrete Fourier transform," *IEEE Transactions on Communication Technology*, vol. 19, no. 5, pp. 628–634, 1971.

[15] G. van Kempen and L. van Vliet, "Mean and variance of ratio estimators used in fluorescence ratio imaging," *Cytometry*, vol. 39, no. 4, pp. 300–305, 2000.

[16] V. Erceg, K. V. S. Hari, M. S. Smith, et al., "Channel models for fixed wireless applications," Tech. Rep. IEEE 802.16a-03/01, July 2003.

Ch. Nanda Kishore received B.Tech. degree in electronics and communication engineering from Jawaharlal Nehru Technological University, Hyderabad, India, in June 2000. He joined Hellosoft India Pvt. Ltd, Hyderbad, India, in July 2000. At Hellosoft, he worked in various projects including digital line echo canceler (LEC), channel coding for GSM/GPRS, PBCC mode of WLAN and physical layer design for Wireless metropolitan area network. He received M.S. degree in communication systems and signal processing from International Institute of Information Technology, Hyderabad, India, in June 2005. Presently he is working in very high bit rate digital subscriber line (VDSL) project. His research interests include wireless communications, digital signal processing, and error-control coding.

V. Umapathi Reddy was on the faculty of IIT, Madras, IIT, Kharagpur, Osmania University and Indian Institute of Science (IISc), Bangalore . At Osmania University, he established the research and training unit for navigational electronics (he was its Founding Director). After retiring from IISc in 2001, he joined the Hellosoft India Pvt. Ltd., as CTO. In June 2003, he moved to International Institute of Information Technology, Hyderabad, as the Microsoft Chair Professor, and returned to Hellosoft as the Chief Scientist in December 2005. He held several visiting appointments with the Stanford University and the University of Iowa. His areas of research have been adaptive and sensor array signal processing, and during the last 10 years he has been focusing on the design of OFDM-based physical layer with applications to DSL, WLAN, and WiMax modems. He was on the editorial boards of Indian Journal of Engineering and Materials Sciences, and Proceedings of the IEEE. He was the Chairman of the Indian National Committee for International Union of Radio Science during 1997–2000. He is a Fellow of the Indian Academy of Sciences, the Indian National Academy of Engineering, the Indian National Science Academy, and the IEEE.

Preliminary call for papers

The 2011 European Signal Processing Conference (EUSIPCO-2011) is the nineteenth in a series of conferences promoted by the European Association for Signal Processing (EURASIP, www.eurasip.org). This year edition will take place in Barcelona, capital city of Catalonia (Spain), and will be jointly organized by the Centre Tecnològic de Telecomunicacions de Catalunya (CTTC) and the Universitat Politècnica de Catalunya (UPC).

EUSIPCO-2011 will focus on key aspects of signal processing theory and applications as listed below. Acceptance of submissions will be based on quality, relevance and originality. Accepted papers will be published in the EUSIPCO proceedings and presented during the conference. Paper submissions, proposals for tutorials and proposals for special sessions are invited in, but not limited to, the following areas of interest.

Areas of Interest

- Audio and electro-acoustics.
- Design, implementation, and applications of signal processing systems.
- Multimedia signal processing and coding.
- Image and multidimensional signal processing.
- Signal detection and estimation.
- Sensor array and multi-channel signal processing.
- Sensor fusion in networked systems.
- Signal processing for communications.
- Medical imaging and image analysis.
- Non-stationary, non-linear and non-Gaussian signal processing.

Submissions

Procedures to submit a paper and proposals for special sessions and tutorials will be detailed at www.eusipco2011.org. Submitted papers must be camera-ready, no more than 5 pages long, and conforming to the standard specified on the EUSIPCO 2011 web site. First authors who are registered students can participate in the best student paper competition.

Important Deadlines:

Proposals for special sessions	15 Dec 2010
Proposals for tutorials	18 Feb 2011
Electronic submission of full papers	**21 Feb 2011**
Notification of acceptance	23 May 2011
Submission of camera-ready papers	6 Jun 2011

Webpage: www.eusipco2011.org

Organizing Committee

Honorary Chair
Miguel A. Lagunas (CTTC)

General Chair
Ana I. Pérez-Neira (UPC)

General Vice-Chair
Carles Antón-Haro (CTTC)

Technical Program Chair
Xavier Mestre (CTTC)

Technical Program Co-Chairs
Javier Hernando (UPC)
Montserrat Pardàs (UPC)

Plenary Talks
Ferran Marqués (UPC)
Yonina Eldar (Technion)

Special Sessions
Ignacio Santamaría (Unversidad de Cantabria)
Mats Bengtsson (KTH)

Finances
Montserrat Nájar (UPC)

Tutorials
Daniel P. Palomar (Hong Kong UST)
Beatrice Pesquet-Popescu (ENST)

Publicity
Stephan Pfletschinger (CTTC)
Mònica Navarro (CTTC)

Publications
Antonio Pascual (UPC)
Carles Fernández (CTTC)

Industrial Liaison & Exhibits
Angeliki Alexiou (University of Piraeus)
Albert Sitjà (CTTC)

International Liaison
Ju Liu (Shandong University-China)
Jinhong Yuan (UNSW-Australia)
Tamas Sziranyi (SZTAKI -Hungary)
Rich Stern (CMU-USA)
Ricardo L. de Queiroz (UNB-Brazil)